Environmental Science & Technology

Article

pubs.acs.org/est

Microscale Characterization of Sulfur Speciation in Lake Sediments

Teng Zeng,[†] William A. Arnold,[†] and Brandy M. Toner*[,‡]

[†]Department of Civil Engineering, University of Minnesota, 500 Pillsbury Drive Southeast, Minneapolis, Minnesota 55455, United States

[‡]Department of Soil, Water, and Climate, University of Minnesota, 1991 Upper Buford Circle, St. Paul, Minnesota 55108, United States

Supporting Information

ABSTRACT: Prairie pothole lakes (PPLs) are naturally sulfur-enriched wetlands in the glaciated prairie region of North America. High sulfate levels and dynamic hydrogeochemistry in combination render PPLs a unique environment to explore the speciation of sedimentary sulfur (S). The goals of this research were to define and quantify the solid-phase S pools in PPL sediments and track seasonal dynamics of S speciation. A quantitative X-ray microprobe method was developed based on S 1s X-ray absorption near-edge structure (XANES) spectroscopy and multienergy X-ray fluorescence mapping. Three S pools—pyritic S, reduced organic S (organic mono- and disulfide), and oxidized S (inorganic sulfate, ester sulfate, and sulfonate)—were identified in PPL sediments. No significant seasonal variation was evident for total S, but S speciation showed a seasonal response. During the spring—summer transition, the reduced organic S decreased from 55 to 15 mol %, with a concomitant rise in the oxidized S. During the summer—fall transition, the trend reversed and the reduced organic S grew to 75 mol % at the expense of the oxidized S. The pyritic S, on the other hand, remained relatively constant (~22 mol %) over time. The seasonal changes in S speciation have strong potential to force the cycling of elements such as mercury in prairie wetlands.

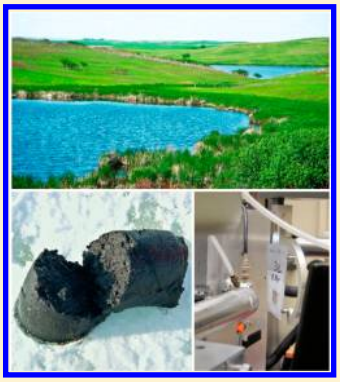

INTRODUCTION

The Prairie Pothole Region (PPR), which extends from northwestern Iowa in the United Sates into central Alberta in Canada, features numerous small, shallow water basins typically referred to as prairie pothole lakes (PPLs).[1] These potholes and related aquatic ecosystems comprise one of the largest grassland ecoregions on Earth and play a prominent role in sustaining the biodiversity and productivity of the PPR.[1] Since their formation during the late Pleistocene glaciation, PPLs have experienced long-term hydrogeochemical evolution.[2,3] High levels of sulfate are frequently detected in PPL water columns,[2,4−6] which has been ascribed to recharge by oxygenated groundwater circulating through pyrite-bearing glacial till over long periods of time.[7,8] Microbially driven sulfate reduction is postulated as a key process in PPLs.[9−11] Field observations have also confirmed that anoxic sediments in PPLs support microbial communities involved in sulfate reduction.[12] Thus, PPL sediments potentially serve as an important reservoir for sulfur (S), and S speciation is likely to be temporally variable due to the dynamic nature of PPLs.[12]

A holistic picture of S cycling in PPLs is essential to evaluating the ecosystem functions of these water bodies for several reasons. First, several studies concerned with mercury (Hg) occurrence in the PPR have measured elevated concentrations of methylmercury (MeHg) in water sampled from diverse prairie wetlands as well as invertebrates in these systems.[13−15] In anoxic sediments, sulfate-reducing microorganisms stimulate Hg methylation to form MeHg.[16−18] Meanwhile, reduced organic S represents a major pool of high-affinity binding sites for both Hg and MeHg.[19−27] Characterization of S speciation dynamics in PPL sediments, therefore, is of indisputable relevance for predicting the methylation rate, mobility, and bioavailability of mercury in prairie wetlands. Second, PPL water levels fluctuate widely in response to interannual and intraannual wetting and drying cycles,[28] which has been recognized as the sensitivity of prairie ecosystems to climate variability.[29] Low water and occasional drying of the lake bottom may expose previously anoxic sediments to oxygen,[9] causing the dissolution of sulfide minerals such as pyrite upon reoxidation.[10,30,31] Assessing likely consequences of such processes, mainly leaching of acidity and heavy metals, requires knowledge of S speciation in PPLs. Third, the landscape of the PPR has been severely altered by extensive historical and ongoing drainage of PPLs associated with expanding agricultural activity.[32] Remaining and restored PPLs often trap nonpoint source pollutants, particularly pesticides and fertilizers, from adjacent farmland.[33−36] The redox-active entities present in PPL sediments, most likely sulfide minerals, can promote the abiotic degradation of pesticides.[37] Hence, an improved understanding of the identity and abundance of reactive S species in PPL sediments would reveal new insights into the natural attenuation of pesticides. Fourth, recent research has demonstrated that prairie wetlands

Received: September 26, 2012
Revised: December 13, 2012
Accepted: January 2, 2013
Published: January 2, 2013

are landscape-scale hotspots for methane emissions.[38−40] The release of methane from PPLs is strongly correlated with sulfate reduction in sediments, which is thought to trigger the onset of methane production.[39,40] Elucidating S speciation in PPL sediments is not only crucial for accounting for the effect of S cycling on methane fluxes across the prairie landscape but also the development of regionally specific assessments on the net greenhouse gas budget.

The speciation of S is a critical determinant of S biogeochemistry. The dynamic cycling of diverse reduced and oxidized S forms (i.e., ranging from −2 in sulfide to +6 in sulfate) in sedimentary environments involves a complex interplay of sulfate reduction, diagenetic S interconversion, and biogenic S deposition.[41−43] Existing knowledge of S in geochemical materials heavily relies on the application of selective sequential extraction methods, which provide a useful but operationally defined view of solid-phase S rather than direct speciation data.[44] Furthermore, extraction-based methods are prone to artifacts associated with sample integrity loss and reagent selectivity.[45,46] Synchrotron-based X-ray absorption near-edge structure (XANES) spectroscopy has, in recent years, emerged as a nondestructive and element-sensitive technique for describing the speciation and distribution of S and other elements at the microscale.[47] Despite the utility of S 1s XANES spectroscopy, only one study has applied this technique to semiquantitatively describe the solid-phase S speciation in hydric prairie wetland soils.[31]

Previous environmental applications of XANES analyses have mainly focused on (1) determining the bulk average speciation of an element for a sample (i.e., bulk spectroscopy) or (2) examining elemental speciation at a point location within a sample using a microprobe instrument (i.e., point spectra). Neither approach adequately captures the heterogeneity of elemental speciation present within a complex sample.[48,49] One key objective of this study was to quantify the S species in PPL sediments by developing a S chemical mapping protocol that integrates multienergy X-ray fluorescence (XRF) mapping with point XANES spectra to ground truth the chemical map. For each sample, XRF maps were collected at multiple energies spanning the S 1s absorption edge. Individual XRF maps were then aligned to create a composite S chemical map having a seven-point absorption spectrum at each pixel within the area of interest. The S chemical maps were fit with reference XANES spectra of identified S species to extract quantitative information on S speciation. A similar approach has recently been applied to quantify the iron speciation in heterogeneous geochemical samples such as water-rock reaction media,[48] suspended marine particulates,[49] hydrothermal plume particles,[50] and oceanic crust.[51]

EXPERIMENTAL SECTION

Sample Collection and Preparation. A series of lake sediment cores were collected from two adjacent PPLs (Lakes P1 and P8) in the U.S. Geological Survey (USGS) Cottonwood Lake study area, Jamestown, ND [Supporting Information (SI), Figure S1], during January, April, June, and September 2010 (hereafter referred to as P1Jan/Apr/Jun/Sep and P8Apr/Sep). Further descriptions of the site, core collection and processing, and sediment sample preparation for S XANES spectroscopy are provided in the SI.

XRF Mapping and XANES Spectra Acquisition. Acquisition of XRF maps and XANES spectra was performed at the microprobe beamline 10.3.2 of the Advanced Light Source, Lawrence Berkeley National Laboratory (Berkeley, CA),[52] during November 2011 and May 2012.

During the 2011 analyses, samples P1Sep and P8Sep were analyzed to obtain baseline information about the major S species in PPL sediments. XRF maps were acquired by scanning a 2000 μm × 1000 μm region of interest on samples at two incident X-ray beam energies of 2472.8 and 2482.5 eV using a Si(111) double crystal monochromator with a beam spot size of 15 μm (horizontal) × 6 μm (vertical).[52] These two energies were chosen to represent the white-line peaks of common reduced and oxidized S species, respectively. The absolute energy of the monochromator was periodically calibrated against the white-line peak of gypsum (2482.74 eV) at a precision of 0.15 eV. The sample holder was mounted at a 45° angle to the incident beam, and the signal was recorded at an angle of 90° using a seven-element germanium detector in fluorescence mode.[52] Samples were run with helium in the I_0 chamber to minimize the beam attenuation by air.[52] Counts in 15 spectral regions of interest were recorded for each map, including S (2120−2350 eV). The distance of the detector relative to the sample was finely adjusted for optimal S counts. The fluorescence signal was collected for each pixel of the map with a scan step of 8 μm × 8 μm, a dwell time of 120 ms, and a monochromator settling time of 500 ms between horizontal scan lines. For each sample, both XRF maps were deadtime corrected, resized, registered, and stacked to create a single dual-energy composite S map using custom beamline software.[52] The composite S maps were subsequently used to identify S-rich points of interest (POIs, bright and diffused spots with S counts >2000) for XANES scans. For each POI, at least two XANES scans were acquired in the energy range between 2420 and 2625 eV, with a 0.2 eV step size in the XANES region (2465−2486 eV) and coarser step sizes (1 and 2 eV) in the pre-edge and post-edge regions. Examination of successive scans acquired at the same POI showed no apparent changes in spectral shape, thereby suggesting the negligible radiation damage of samples.

During the 2012 analyses, multienergy XRF maps for samples P1Jan, P1Apr, P1Jun, and P1Sep were acquired by sequentially scanning a 1000 μm × 1000 μm region of interest at seven incident beam energies across the S 1s (2466, 2472.2, 2473.5, 2478.5, 2481.2, 2482.6, and 2520 eV). The lowest (2466 eV) and highest (2520 eV) energies were used to determine the background and total counts in the S channel. This approach generates an energy-dependent absorption profile at each pixel within the region of interest and will be referred to as "chemical mapping". The five intermediate energies were selected using an error estimator program to best distinguish spectral features of different S species based on the XANES spectra acquired on P1Sep and P8Sep samples during the 2011 analyses (detailed below). The resulting multienergy S chemical maps for each sample were used to guide the selection of S-rich POIs on which to acquire XANES spectra as described above. For comparison purposes, S chemical maps for samples P8Apr and P8Sep were also acquired for a 600 μm × 600 μm region of interest.

For the acquisition of S reference XANES spectra, a thin layer of finely ground S compound was spread onto a conductive graphite tape and the signal was recorded in total electron yield mode to minimize overabsorption effects.[53] Reference XANES spectra were collected for eight S compounds [i.e., 1-amino-2-naphthol-4-sulfonic acid (ANSA), L-cysteine, DL-homocysteic acid, L-methionine, DL-methionine

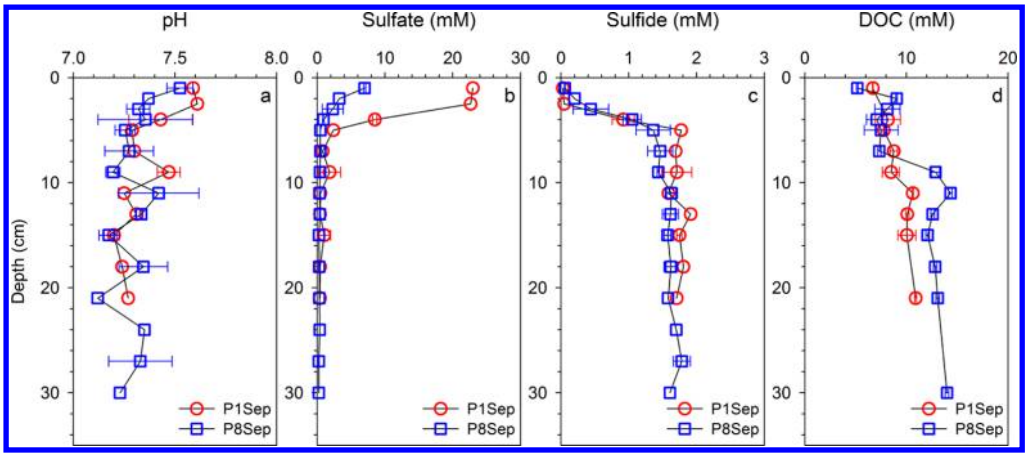

Figure 1. Depth profiles of pH, sulfate, sulfide, and DOC for P1Sep and P8Sep sediment porewater samples. The sediment–water interface is dictated by "0 cm". Error bars represent one standard deviation of duplicate samples; where absent, only one sample was analyzed. DOC data were averaged from values reported by Ziegelgruber.[67]

sulfoxide, sodium dodecyl sulfate (SDS), sulfanilamide, and 2-thiophenecarboxylic acid]. These spectra were compiled with seven donated spectra (i.e., L-cystine, elemental sulfur, greigite, mackinawite, pyrite, sodium sulfite, and sodium thiosulfate[54,55]) to generate a reference database that was used for fitting XANES spectra and chemical maps. Of the donated spectra, only greigite, mackinawite, and sodium thiosulfate were collected on a different beamline and reprocessed for use.[54] The selected S reference compounds exhibited distinct spectral features (e.g., energies and intensity of white-line peaks) relative to one another and represent the S species frequently encountered in sedimentary environments (Table S1 and Figures S2 and S3, SI).

XRF Map and XANES Spectra Analysis. All experimental S XANES spectra were deadtime corrected and energy calibrated, followed by the preedge background subtraction (2420–2466 eV) and step-edge height normalization to unity (2520–2625 eV). Normalized spectra were submitted to a principal component analysis (PCA) using SixPACK[56] following previously published protocols.[57] The number of spectral components present in sample XANES spectra was evaluated with the local minimum IND value (an indicator for the number of components used for fitting) and the quality of reconstruction of the S reference spectra by target transformation with the SPOIL value (an indicator for the increase in the fit error when replacing a component),[53,58,59] which provides a statistical basis for defining the most appropriate subset of S references for spectral fitting.[60] Reference compounds with smaller SPOIL values were ranked as the high priority predictors for subsequent least-squares linear combination fittings (LCF). The fitting of XANES spectra was performed with linear combinations of reference spectra over the energy range of 2460–2560 eV using custom beamline software,[61] with the sum of the total S species not constrained to unity and minor energy shifts permitted (±0.3 eV). The fit quality was evaluated with the normalized sum-squared residual (NSS), and the addition of a component was justified when NSS decreased by at least 10%. The quantification error was estimated to be ±10 mol % after accounting for uncertainties associated with data collection and reduction as well as the spectral representativeness of the chosen S reference compounds.[55,62] The results of the best fit were taken to indicate the S oxidation state and functional moiety rather than actual specific S-bearing compounds.

For quantitative chemical mapping analyses, multienergy S chemical maps were fitted using S reference spectra along with a background spectrum from a sample blank (XRF tape and Mylar X-ray film). The fitting procedure essentially took a seven-point XANES spectrum at each pixel in the map and fit that spectrum with a linear combination of the seven-point XANES spectra of the reference compounds.[63] The fit quality was evaluated with the whole-map mean squared error. A conservative error estimate of ±10 mol % was calculated using custom beamline software based on the degree to which normalized absorption differed for S reference spectra at the chemical map energies used. The total count of each S species was calculated by summing the counts from all pixels in the corresponding chemical map channel and normalized by the mapping area. The area-normalized counts were further corrected by subtracting the background counts from sediment-free areas of the prepared sample. The background-subtracted counts were converted to the relative proportion of each S species in the map.

RESULTS AND DISCUSSION

Chemistry of PPL Surface Water, Sediment Porewaters, and Sediments. The chemistry of bulk surface water and sediment porewaters from P1 and P8 has been previously characterized[6,37,64] and selected results are presented in Table S2 (SI). In general, PPL surface water contained high sulfate (5–30 mM) with pH ~8.0. Hydrogen sulfide and dissolved iron were nondetectable. PPL sediment porewaters had a similar pH range and contained high sulfide levels (0.9–2.4 mM) but low sulfate (0.4–1.0 mM). Elevated concentrations of polysulfides, sulfite, and thiosulfate have also been measured in the porewaters.[37] The dissolved organic carbon (DOC) concentrations in porewaters (6–10 mM) were typically 2–3 times greater than those measured in the surface water (1.8–3.2 mM), while the dissolved iron was low (<1 μM). A selection of depth profiles (pH, sulfate, sulfide, and DOC) is presented in Figure 1 for P1Sep and P8Sep sediment porewaters. The porewater pH was near neutral (7.0–8.0) for all depths. The surficial porewater sulfate concentration (7–23 mM) fell in the same range with overlying water, but decreased with increasing depth and stayed consistently low (<1.0 mM)

dx.doi.org/10.1021/es303914q | Environ. Sci. Technol. 2013, 47, 1287–1296

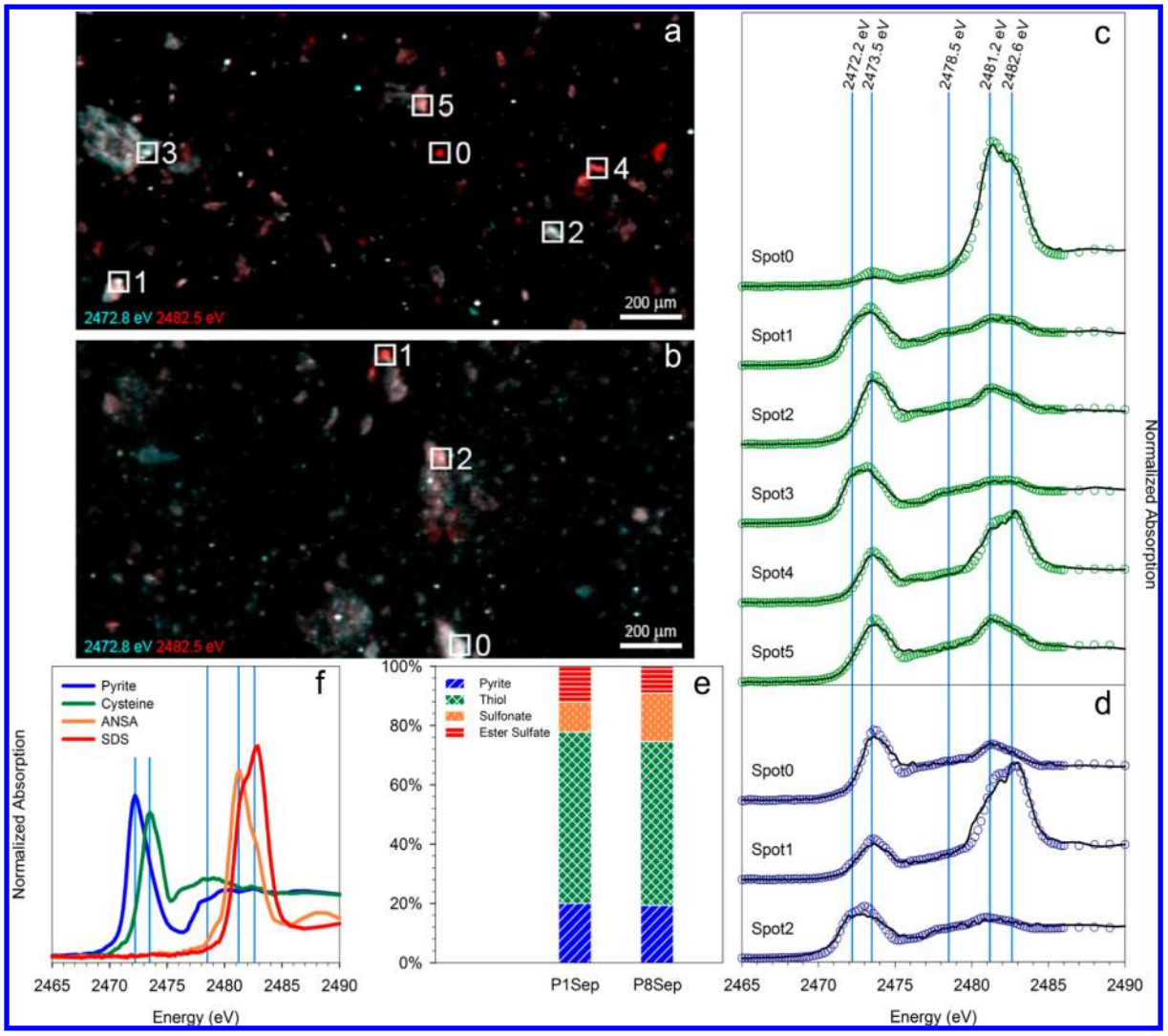

Figure 2. Identification of major S species in P1Sep and P8Sep sediment samples: (a and b) bicolor composite S maps (energies at 2472.8 and 2482.5 eV) of P1Sep and P8Sep, respectively; (c and d) XANES spectra and LCF analyses of POIs on P1Sep and P8Sep, respectively; (e) fractional contribution of S species calculated from the LCF analyses of averaged XANES spectra of P1Sep and P8Sep, respectively, with the sum of all S species normalized to 100 mol % (Table S6, SI); and (f) overplot of XANES spectra of four S reference compounds. Light blue lines in panels c, d, and f dictate five intermediate mapping energies at which S chemical maps were scanned.

below ~10 cm. The porewater sulfide front showed an inverse trend, reaching its near-maximum by ~5 cm and remaining relatively constant downward. Similarly, the porewater DOC concentration displayed a downcore increase with a median of 9.5 mM. The disappearance of porewater sulfate with a progressive increase of sulfide indicates that sulfate reduction commenced at the top few centimeters of the sediment−water interface. Below 10 cm in depth, however, the depletion of sulfate coupled with the saturation of sulfide signifies that sulfate reduction was inhibited, and methanogenesis might dominate the organic matter mineralization.[65,66] Collectively, porewater redox zonation suggests that suboxic conditions existed within the near-surface portion while anoxic conditions persisted throughout the deeper layers of PPL sediments. The chemistry of bulk P1 and P8 sediments is summarized in Table S3 (SI). All sediment samples were characterized by high total S (12.5−13.4 g/kg) and organic carbon content (262−269 g/kg), which fall at the upper end of the data range reported for other lake sediments.[41] Given the high S/C ratio (~0.05) and iron content (~1.8 wt %), both organic S and iron sulfide species were expected to constitute the bulk of S in PPL sediments (see the SI for additional discussion).

Energy Optimization for Chemical Mapping. Figure 2 presents the dual-energy composite S maps and XANES spectra of P1Sep and P8Sep sediment samples. Within a distance of several hundred micrometers, the S aggregates vary between dominantly oxidized and reduced S species (Figure 2a,b), which calls for the need to apply chemical mapping capable of representing the heterogeneity of S speciation within a sample. The S XANES spectra typically contain two distinct absorption bands, mainly corresponding to the reduced S and the highly oxidized S (Figure 2c,d). The first band near the 2470−2475 eV region could be assigned to inorganic (e.g., pyrite) and/or organic (e.g., thiol) reduced S species, while the second band near the 2480−2485 eV region probably originated from highly oxidized S species (e.g., sulfonate or sulfate). Other intermediate S species might also exist in the samples as locally concentrated minor components that could not be resolved from the major features in these spectra. Earlier research using S XANES has identified various inorganic and organic S species

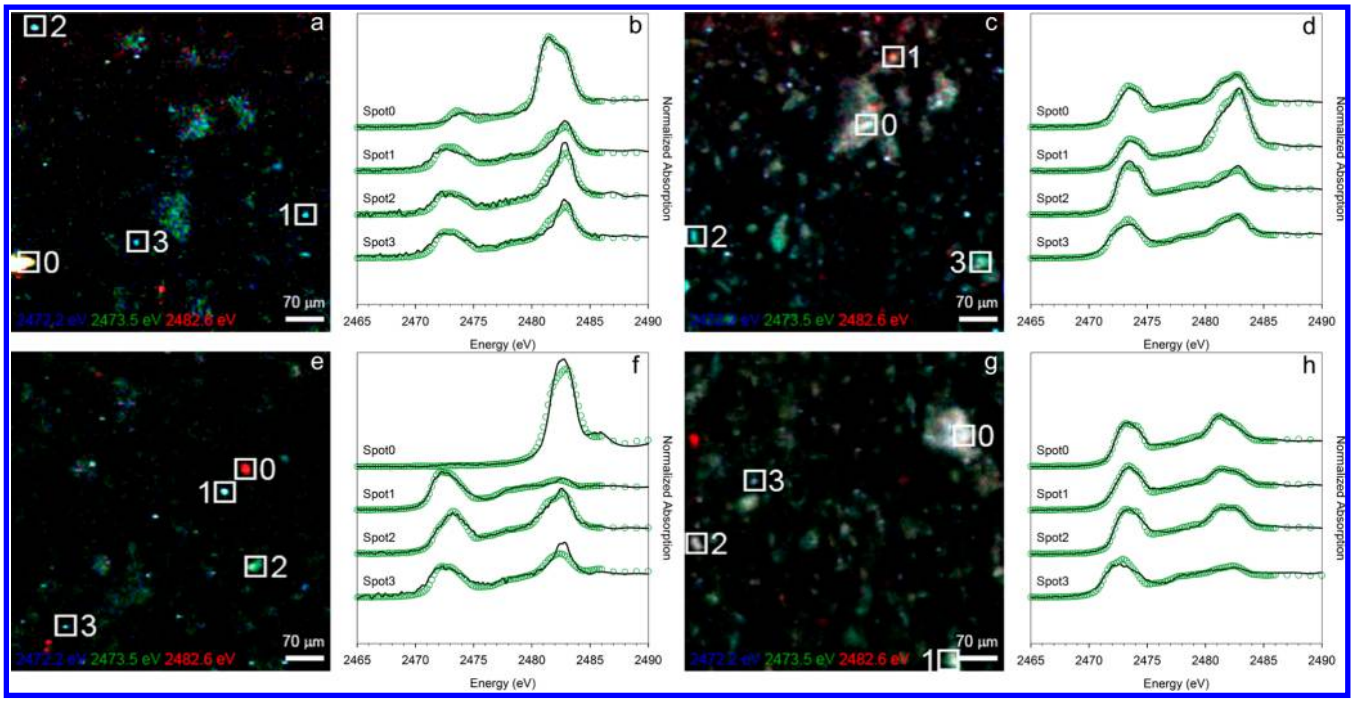

Figure 3. Multienergy S chemical maps and XANES spectra of P1 sediment samples: (a, c, e, and g) tricolor multienergy S chemical maps (energies at 2472.2, 2473.5, and 2482.6 eV) of P1Jan, P1Apr, P1Jun, and P1Sep, respectively, and (b, d, f, and h) XANES spectra and LCF analyses of POIs on P1Jan, P1Apr, P1Jun, and P1Sep, respectively.

in soils and sediments as well as their organic matter extracts (Table S4, SI). Such variation in S species was also supported by results from PCA-target transformation analyses of the P1Sep and P8Sep samples (Table S5, SI).

To derive quantitative information about different S species present, XANES spectra were fit using a suite of S reference spectra (Table S6, SI). In this context, it is noted that the S reference compounds used in LCF only function as proxies for different S functional groups, and the quantitative analysis of an XANES spectrum aims to estimate the fractional contribution of these functional groups rather than individual compounds in a sample. Thus, a satisfactory fit does not necessarily imply that the chosen reference compounds actually exist in the sample, whereas a poor fit may indicate the presence of additional S species that are not well represented by the reference compounds used. Knowledge of the sediment chemistry along with PCA-target transformation analysis makes this database-dependent approach more robust. According to the LCF analyses of XANES spectra (Figure 2e), the P1Sep sample contained significant thiol (58 mol %) and a lesser proportion of pyrite (20 mol %). The oxidized S was less abundant than the reduced S and characterized by sulfonate (10 mol %) and ester sulfate (12 mol %). The dominant S species in the P8Sep sample were not statistically different from those found in P1Sep and consisted of thiol (55 mol %), pyrite (19 mol %), sulfonate (16 mol %), and ester sulfate (9 mol %). The types of S species identified herein corroborate findings from an earlier study characterizing hydric prairie wetland soils, which suggested that pyrite and organic monosulfide comprised the main portion of the reduced S, while sulfonate and inorganic sulfate constituted a significant fraction of the oxidized S.[31] Consequently, the white-line peaks of pyrite (2472.2 eV), cysteine (2473.5 eV), ANSA (2481.2 eV), and SDS (2482.6 eV) along with an intermediate energy (2478.5 eV) were chosen for use in the subsequent multienergy S chemical mapping (Figure 2f).

Seasonal Dynamics of Sulfur Speciation. One particular goal of this research was to quantify the S pools in the sediments of PPLs. To track the seasonal dynamics of S speciation in PPL sediments, XRF maps were collected at seven incident energies for both P1 and P8 sediment samples, with XANES scans acquired on four P1 samples to ground truth chemical map fit results. Figure 3 presents the multienergy S chemical maps and XANES spectra of P1Jan, P1Apr, P1Jun, and P1Sep samples. The PCA-target transformation analyses of XANES spectra are summarized in Table S7 (SI). Results on S speciation from the fits to chemical maps (Table S8, SI) and XANES spectra (Table S9, SI) are compiled in Table S10 (SI). The chemical map results for the P8Apr and P8Sep samples (Table S10 and Figure S4, SI) show similar S speciation patterns as for the P1 samples.

According to the chemical map fitting and S XANES verification of the fit results, three basic S pools were identified: (1) pyritic S, (2) reduced organic S, and (3) oxidized S. The "pyritic S" pool contained S with spectral properties consistent with pyrite. The "reduced organic S" pool consisted of S with spectral properties consistent with organic monosulfide (cysteine as the reference material) and disulfide (cystine as the reference material) and will be referred to as "reduced org-S" in the following discussion. The "oxidized S" pool consisted of S with spectral properties consistent with inorganic sulfate (gypsum as the reference material) and ester sulfate (SDS as the reference material). For simplicity, the rarer sulfonate signals (<10 mol % in just two samples) observed were totaled with sulfate in the oxidized S pool during interpretation of the S chemical mapping data [Table S10 (SI) and Figure 4].

At P1, although the sediment total S and total organic carbon stayed relatively constant, the chemical mapping data reveal that S speciation changed as a function of season. Of the three S

dx.doi.org/10.1021/es303914q | Environ. Sci. Technol. 2013, 47, 1287−1296

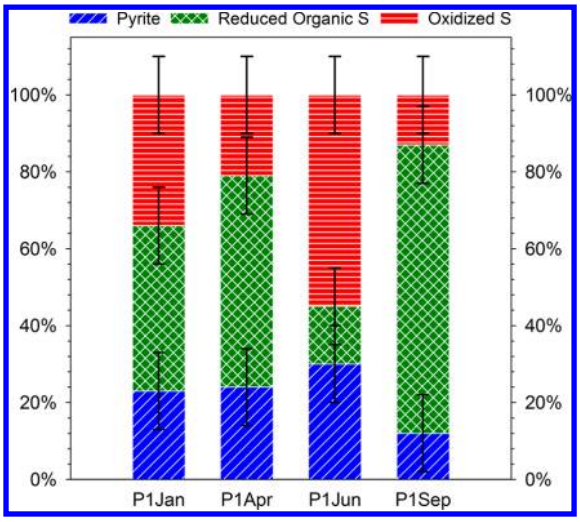

Figure 4. Fractional contribution of pyrite, reduced organic S, and oxidized S in the P1 sediment samples with the sum of all S species normalized to 100 mol %. Stacked bars plotted on the basis of data in Table S10 (SI). Error bars represent an error estimate of ±10 mol %.

pools—pyrite, reduced org-S, and oxidized S—only pyrite remained constant within the ±10 mol % error estimate for the four samples over the year. When all data are considered, the results offer compelling evidence for major exchange between two S pools, reduced org-S and oxidized S, on a seasonal scale [Figure 4 and Table S10 (SI)]. During the winter−spring transition (P1Jan to P1Apr), the reduced org-S pool increased (from 43 ± 10 to 55 ± 10 mol %) and was accompanied by a decrease of similar magnitude in the oxidized S pool (from 34 ± 10 to 21 ± 10 mol %). During the spring−summer transition (P1Apr to P1Jun), the reduced org-S pool declined sharply (from 55 ± 10 to 15 ± 10 mol %) while the oxidized S pool increased (from 21 ± 10 to 55 ± 10 mol %). During the summer−fall transition (P1Jun to P1Sep), the reduced org-S pool grew significantly (from 15 ± 10 to 75 ± 10 mol %) at the expense of the oxidized S pool (from 55 ± 10 to 13 ± 10 mol %). Seasonal variation in S speciation within P1 sediments may be, at least in part, regulated by sulfate reduction, especially during the summer−fall transition. The sulfate reduction rate (SRR) is closely coupled to temperature, the supply of labile organic matter, as well as the redox status of sediments,[68−75] and increases in the SRR are often out of phase with the accumulation of reduced S.[74,76−78] Specifically, the SRR peaks in the summer due to elevated temperature and/or higher availability of organic substrates after the spring bloom, while the accumulation of reduced S only becomes apparent later in the fall.[74,76,78] Most studies advocate fast reoxidation of sulfide during the summer, mainly promoted by the intensified downward diffusion of dissolved oxygen into surficial sediments,[79,80] as a likely cause for the observed seasonal delay.[71,73,81,82] A similar scheme may hold for the seasonality of S speciation in P1 sediments. Further evidence comes partly from the fact that the sulfide concentration in the bulk P1Sep sediment porewaters doubled that measured in the P1Jun porewaters (Table S2, SI). The current study thus highlights the need to further constrain the redox-induced cycling of S in PPLs by tracking the temporal trend of the SRR.

Pyritic Sulfur Pool. Pyrite (FeS_2) was a primary contributor to the reduced S in PPL sediments, suggesting that the sequestration by reactive iron was an important S sink. Pyrite ubiquitously occurs in riverine,[54] lacustrine,[83,84] estuarine,[85] and marine sediments.[86−88] Although a detrital origin of sedimentary pyrite is possible,[84] its prevalence is more likely explained by diagenetic reactions involving hydrogen sulfide or polysulfides.[89] The presence of pyrite in hydric prairie wetland soils was previously shown, but its relative abundance to reduced org-S species was unresolved.[31] It should be pointed out that iron−thiolate complexes (Fe−S−R) found in metalloproteins of organisms may produce spurious features of iron sulfides in XANES spectra.[90,91] Thus, the fit results for pyrite in this study must be interpreted with caution in the absence of detailed mineralogical characterization. While the magnitude of the pyrite pool in PPL sediments did not change appreciably, the S chemical mapping and XANES data are not sufficient to conclude that the pool was unreactive over the course of the study.

Reduced Organic Sulfur Pool. Thiol (R−S−H) and disulfide (R−S−S−R′) were the quantitatively dominant reduced org-S in PPL sediments. Previous studies on estuarine and marine sediments as well as hydric prairie wetland soils have documented that organic sulfides (e.g., thiol, mono-, di-, and polysulfides) contribute up to 70% of the total S.[31,83,85,88] In sedimentary environments, thiols form via the addition of hydrogen sulfide or polysulfides onto functionalized organic matter[92] and undergo intermolecular reactions to form organic monosulfide (R−S−R′).[93] Thiol and organic monosulfide may also originate from decaying organic matter due to their ubiquity in living organisms (e.g., amino acids cysteine and methionine).[94,95] On the other hand, organic disulfide can form through the intermolecular cross-linking of two thiol groups upon oxidation.[96] The strength and rigidity of such disulfide cross-linking likely enhance the stability of organic matter.[97,98] It should be noted that the S 1s XANES does not allow an assessment of the relative amounts of thiol and organic monosulfide in the reduced org-S pool because of their similar white-line peaks and spectral features (Figures S2 and S3, SI).[99] In this study, the inclusion of both species in the LCF caused one to increase and the other to decrease simultaneously. Thus, the fit results derived from cysteine should be interpreted as the joint contribution from thiol and organic monosulfide.

Oxidized Sulfur Pool. Sulfate was the principal oxidized form of S found in PPL sediments. Previous research has mainly detected ester sulfate ($R-O-SO_3^-$) in lacustrine,[84] estuarine,[85] and marine sediments.[87,88] Inorganic sulfate (SO_4^{2-}), however, seemed to predominate hydric prairie wetland soils (39−43%).[31] In sedimentary environments, sulfate may exist in multiple forms, including ester sulfate, inorganic sulfate, and carbonate-hosted sulfate, and each of these is differentiated by subtle differences in their XANES spectra.[100] More specifically, ester sulfate exhibits a splitting in its white-line peak induced by the asymmetry of S coordination environment, while carbonate-hosted and inorganic sulfate have a more symmetric white-line peak but exhibit additional features in the postedge region.[83,101] Although SDS typically yielded better fits than gypsum in this study, the inclusion of both species in the P1Jan and P1Jun samples improved the fitting quality, pointing to the coexistence of ester and inorganic sulfate.

Sulfonate was only present in the P1Sep and P8Sep samples as a minor component of oxidized S. The widespread occurrence of sulfonate in marine and estuarine sediments has been reported.[85,87,88,93] Significant amounts of sulfonate have also been identified in hydric prairie wetland soils (17−

31%).[31] Sulfonate has various biochemically important structural analogues in living organisms (e.g., amino sulfonic acid taurine) and may be directly introduced into sediments from decaying organic matter.[85,87] Alternatively, sulfonate may form upon the oxidation of thiol or organic disulfide or the reaction of sulfite or thiosulfate with organic matter.[88,102] Unlike organic sulfides, which are often associated with highly labile organic matter, sulfonate tends to associate with less labile phases of organic matter and is more resistant to mineralization or transformation.[103] In this study, the low abundance of sulfonate in PPL sediment samples is presumably consistent with either low production or rapid consumption and does not provide clear evidence for its importance.

Environmental Implications. One of the major weaknesses of microprobe techniques is the uncertainty in making representative observations; therefore, quantification has been difficult or impossible. Because the goal for this study was to *quantify*, not just describe, the changes in S speciation among samples, the need for a greater number of representative observations was clear. As a result of the chemical mapping approach developed, the number of observations (n) improved from n = 5−10 (point XANES) to n > 400 000 (points in a single chemical map), thereby creating a more complete picture of the S composition of a sample. In practice, the chemical mapping approach also yields point XANES, which are used to validate the chemical map rather than representing a standalone data set. As a leap forward from the standard bulk XANES, the chemical mapping adds a new dimension to capturing the within sample variability, in that both locally concentrated and diffusely spread S species can be spatially resolved yet instantly and intimately coupled. The development of micro-XAS tools that can describe elemental speciation in naturally heterogeneous materials, as well as provide quantification, indicates that these synchrotron-based approaches are now ready to contribute to major advances in the field of biogeochemistry.

In regard to S biogeochemical cycling in PPLs, the seasonality of S speciation observed herein could have profound effects on the storage, transformation, and mobilization of contaminants such as Hg in prairie wetlands. For instance, during the spring−summer transition, the sequestration of Hg by reduced org-S may be impeded as organic sulfides become less abundant in PPLs. This release of Hg would immediately precede a large accumulation of sulfate and the onset of the methylating activity of sulfate-reducing microorganisms. Thus, the seasonal S cycling is poised to indirectly regulate Hg inventory in PPLs. The quantification of lake sediment S species achieved in this study provides an essential window into the seasonal variation in S speciation and shows strong potential to unlock our understanding of processes driving other elemental cycles, such as Hg. Further characterization of lake sediments representing a full range of depositional heterogeneities, however, is a necessary prerequisite for unraveling changes in S speciation occurring under differing sedimentation patterns, organic matter load, and redox dynamics. In a broader biogeochemical context, the S chemical mapping approach may find ready application in and facilitate the prediction of S cycling in estuarine and marine sediments and marine water column particles, as well as soils.

■ ASSOCIATED CONTENT

Supporting Information

Additional materials as noted in the text. This material is available free of charge via the Internet at http://pubs.acs.org.

■ AUTHOR INFORMATION

Corresponding Author

*E-mail: toner@umn.edu; phone: 612-624-1362; fax: 612-625-2208.

Notes

The authors declare no competing financial interest.

■ ACKNOWLEDGMENTS

We wish to acknowledge Dr. David N. Mushet (USGS Northern Prairie Wildlife Research Center) and Dr. Yu-Ping Chin and Kate L. Ziegelgruber (School of Earth Sciences, The Ohio State University) for their assistance in field sampling and sample processing. We are also grateful to Dr. Matthew A. Marcus and Dr. Sirine C. Fakra (The Advanced Light Source, Lawrence Berkeley National Laboratory) for synchrotron support and expert guidance. We further wish to thank Jill K. Coleman Wasik (Science Museum of Minnesota), Jeffrey V. Sorensen, Brandi R. Kamermans, and Sarah L. Nicholas (Department of Soil, Water, and Climate, U of MN) for assistance in synchrotron data collection and analysis. We also appreciate the anonymous reviewers for their valuable comments. Special thanks go to Dr. Edward D. Burton (Southern Cross GeoScience, Southern Cross University, Australia) for sharing the S XANES spectra of greigite, mackinawite, and sodium thiosulfate as well as Dr. Kathryn L. Nagy (Department of Earth and Environmental Sciences, University of Illinois at Chicago) and Dr. Alain Manceau (Institute of Earth Science, Université Joseph Fourier) for sharing the S XANES spectra of L-cystine, elemental sulfur, pyrite, and sodium sulfite ahead of publication. This research was funded by the Gordon and Betty Moore Foundation (B.M.T.), the Joseph T. and Rose S. Ling Professorship (W.A.A.), and National Science Foundation grant EAR-0910692 (W.A.A.). The Advanced Light Source is supported by the Director, Office of Science, Office of Basic Energy Sciences, of the U.S. Department of Energy under Contract No. DE-AC02-05CH11231.

■ REFERENCES

(1) van der Valk, A. G. The prairie potholes of North America. In *The World's Largest Wetlands*; Fraser, L. H., Keddy, P. A., Eds.; Cambridge University Press: Cambridge, UK, 2005; pp 393−423.

(2) LaBaugh, J. W. Chemical characteristics of water in northern prairie wetlands. In *Northern Prairie Wetlands*; van der Valk, A. G., Ed.; Iowa State University Press: Ames, IA, 1989; pp 56−90.

(3) Last, W. M.; Ginn, F. M. Saline systems of the Great Plains of western Canada: An overview of the limnogeology and paleolimnology. *Saline Syst.* **2005**, *1*, 1−38.

(4) Last, W. M. Chemical composition of saline and subsaline lakes of the northern Great Plains, western Canada. *Int. J. Salt Lake Res.* **1992**, *1*, 47−76.

(5) Waiser, M. J.; Robarts, R. D. Microbial nutrient limitation in prairie saline lakes with high sulfate concentration. *Limnol. Oceanogr.* **1995**, *40*, 566−574.

(6) Zeng, T.; Ziegelgruber, K. L.; Chin, Y.-P.; Arnold, W. A. Pesticide processing potential in prairie pothole porewaters. *Environ. Sci. Technol.* **2011**, *45*, 6814−6822.

(7) Van Stempvoort, D. R.; Hendry, M. J.; Schoenau, J. J.; Krouse, H. R. Sources and dynamics of sulfur in weathered till, Western Glaciated Plains of North America. *Chem. Geol.* **1994**, *111*, 35−56.

(8) Goldhaber, M. B.; Mills, C. T.; Stricker, C. A.; Morrison, J. M. The role of critical zone processes in the evolution of the Prairie Pothole Region wetlands. *Appl. Geochem.* **2011**, *26* (Supplement), S32−S35.
(9) LaBaugh, J. W.; Winter, T. C.; Swanson, G. A.; Rosenberry, D. O.; Nelson, R. D.; Euliss, N. H., Jr. Changes in atmospheric circulation patterns affect midcontinent wetlands sensitive to climate. *Limnol. Oceanogr.* **1996**, *41*, 864−870.
(10) Heagle, D.; Hayashi, M.; van der Kamp, G. Use of solute mass balance to quantify geochemical processes in a prairie recharge wetland. *Wetlands* **2007**, *27*, 806−818.
(11) Mills, C. T.; Goldhaber, M. B.; Stricker, C. A.; Holloway, J. M.; Morrison, J. M.; Ellefsen, K. J.; Rosenberry, D. O.; Thurston, R. S. Using stable isotopes to understand hydrochemical processes in and around a Prairie Pothole wetland in the Northern Great Plains, USA. *Appl. Geochem.* **2011**, *26* (Supplement), S97−S100.
(12) Biondini, M. E.; Arndt, J. L. *The Biogeochemistry of Carbon, Nitrogen and Sulfur Transformations in Seasonal and Semipermanent Wetlands*; Technical Report No. ND90-05; North Dakota Water Research Institute: Fargo, ND, 1993.
(13) Sando, S. K.; Krabbenhoft, D. P.; Johnson, K. M.; Lundgren, R. F.; Emerson, D. G. *Mercury and Methylmercury in Water and Bottom Sediments of Wetlands at Lostwood National Wildlife Refuge, North Dakota, 2003−04*; Scientific Investigations Report 2007−5219; U.S. Geological Survey: Reston, VA, 2007; pp 1−74.
(14) Hall, B. D.; Baron, L. A.; Somers, C. M. Mercury concentrations in surface water and harvested waterfowl from the prairie pothole region of Saskatchewan. *Environ. Sci. Technol.* **2009**, *43*, 8759−8766.
(15) Bates, L. M.; Hall, B. D. Concentrations of methylmercury in invertebrates from wetlands of the Prairie Pothole Region of North America. *Environ. Pollut.* **2012**, *160*, 153−160.
(16) Gilmour, C. C.; Henry, E. A.; Mitchell, R. Sulfate stimulation of mercury methylation in freshwater sediments. *Environ. Sci. Technol.* **1992**, *26*, 2281−2287.
(17) Benoit, J. M.; Gilmour, C. C.; Mason, R. P.; Heyes, A. Sulfide controls on mercury speciation and bioavailability to methylating bacteria in sediment pore waters. *Environ. Sci. Technol.* **1999**, *33*, 951−957.
(18) Jonsson, S.; Skyllberg, U.; Nilsson, M. B.; Westlund, P.-O.; Shchukarev, A.; Lundberg, E.; Björn, E. Mercury methylation rates for geochemically relevant Hg^{II} species in sediments. *Environ. Sci. Technol.* **2012**, *46*, 11653−11659.
(19) Xia, K.; Skyllberg, U.; Bleam, W. F.; Bloom, P. R.; Nater, E. A.; Helmke, P. A. X-ray absorption spectroscopic evidence for the complexation of Hg(II) by reduced sulfur in soil humic substances. *Environ. Sci. Technol.* **1999**, *33*, 257−261.
(20) Hesterberg, D.; Chou, J. W.; Hutchison, K. J.; Sayers, D. E. Bonding of Hg(II) to reduced organic sulfur in humic acid as affected by S/Hg ratio. *Environ. Sci. Technol.* **2001**, *35*, 2741−2745.
(21) Skyllberg, U.; Xia, K.; Bloom, P. R.; Nater, E. A.; Bleam, W. F. Binding of mercury(II) to reduced sulfur in soil organic matter along upland−peat soil transects. *J. Environ. Qual.* **2000**, *29*, 855−865.
(22) Wolfenden, S.; Charnock, J. M.; Hilton, J.; Livens, F. R.; Vaughan, D. J. Sulfide species as a sink for mercury in lake sediments. *Environ. Sci. Technol.* **2005**, *39*, 6644−6648.
(23) Yoon, S.-J.; Diener, L. M.; Bloom, P. R.; Nater, E. A.; Bleam, W. F. X-ray absorption studies of CH_3Hg^+-binding sites in humic substances. *Geochim. Cosmochim. Acta* **2005**, *69*, 1111−1121.
(24) Skyllberg, U.; Bloom, P. R.; Qian, J.; Lin, C.-M.; Bleam, W. F. Complexation of mercury(II) in soil organic matter: EXAFS evidence for linear two-coordination with reduced sulfur groups. *Environ. Sci. Technol.* **2006**, *40*, 4174−4180.
(25) Skyllberg, U. Competition among thiols and inorganic sulfides and polysulfides for Hg and MeHg in wetland soils and sediments under suboxic conditions: Illumination of controversies and implications for MeHg net production. *J. Geophys. Res.* **2008**, *113*, DOI 10.1029/2008JG000745.
(26) Skyllberg, U.; Drott, A. Competition between disordered iron sulfide and natural organic matter associated thiols for mercury(II)—An EXAFS study. *Environ. Sci. Technol.* **2010**, *44*, 1254−1259.
(27) Nagy, K. L.; Manceau, A.; Gasper, J. D.; Ryan, J. N.; Aiken, G. R. Metallothionein-like multinuclear clusters of mercury(II) and sulfur in peat. *Environ. Sci. Technol.* **2011**, *45*, 7298−7306.
(28) LaBaugh, J. W.; Winter, T. C.; Rosenberry, D. O. Hydrological functions of prairie wetlands. *Great Plains Res.* **1998**, *8*, 17−37.
(29) Johnson, W. C.; Millett, B. V.; Gilmanov, T.; Voldseth, R. A.; Guntenspergen, G. R.; Naugle, D. E. Vulnerability of northern prairie wetlands to climate change. *BioScience* **2005**, *55*, 863−872.
(30) Adamus, P. R. *Condition, Values, and Loss of Natural Functions of Prairie Wetlands of the North-Central United States*; EPA 600-R-92-249; U.S. Environmental Protection Agency: Washington, DC, 1998. http://water.epa.gov/type/wetlands/assessment/appendixb.cfm (Accessed July, 2012).
(31) Jokic, A.; Cutler, J. N.; Ponomarenko, E.; van der Kamp, G.; Anderson, D. W. Organic carbon and sulphur compounds in wetland soils: Insights on structure and transformation processes using K-edge XANES and NMR spectroscopy. *Geochim. Cosmochim. Acta* **2003**, *67*, 2585−2597.
(32) Johnson, R. R.; Oslund, F. T.; Hertel, D. R. The past, present, and future of prairie potholes in the United States. *J. Soil Water Conserv.* **2008**, *63*, 84A−87A.
(33) Neely, R. K.; Baker, J. L., Nitrogen and phosphorous dynamics and the fate of agricultural runoff. In *Northern Prairie Wetlands*, van der Valk, A. G., Ed. Iowa State University Press: Ames, IA, 1989; pp 92−131.
(34) Olness, A.; Staricka, J. A.; Daniel, J. A., Oxidation-reduction and groundwater contamination in the Prairie Pothole region of the Northern Great Plains. In *Water for Agriculture and Wildlife and the Environment—Win−Win Opportunities: Proceedings of the 1996 USCID Wetlands Seminar*; Schaack, J., Anderson, S. S., Eds.; U.S. Committee on Irrigation and Drainage: Denver, CO, 1996; pp 115−131.
(35) Goldsborough, L. G.; Crumpton, W. G. Distribution and environmental fate of pesticides in prairie wetlands. *Great Plains Res.* **1998**, *8*, 73−95.
(36) Detenbeck, N. E.; Elonen, C. M.; Taylor, D. L.; Cotter, A. M.; Puglisi, F. A.; Sanville, W. D. Effects of agricultural activities and best management practices on water quality of seasonal prairie pothole wetlands. *Wetlands Ecol. Manage.* **2002**, *10*, 335−354.
(37) Zeng, T.; Chin, Y.-P.; Arnold, W. A. Potential for abiotic reduction of pesticides in prairie pothole porewaters. *Environ. Sci. Technol.* **2012**, *46*, 3177−3187.
(38) Gleason, R. A.; Tangen, B. A.; Browne, B. A.; Euliss, N. H., Jr. Greenhouse gas flux from cropland and restored wetlands in the Prairie Pothole Region. *Soil Biol. Biochem.* **2009**, *41*, 2501−2507.
(39) Pennock, D.; Yates, T.; Bedard-Haughn, A.; Phipps, K.; Farrell, R.; McDougal, R. Landscape controls on N_2O and CH_4 emissions from freshwater mineral soil wetlands of the Canadian Prairie Pothole region. *Geoderma* **2010**, *155*, 308−319.
(40) Badiou, P.; McDougal, R.; Pennock, D.; Clark, B. Greenhouse gas emissions and carbon sequestration potential in restored wetlands of the Canadian prairie pothole region. *Wetlands Ecol. Manage.* **2011**, *19*, 237−256.
(41) Urban, N. R., Retention of sulfur in lake sediments. In *Environmental Chemistry of Lakes and Reservoirs*; Baker, L. A., Ed.; American Chemical Society: Washington, DC, 1994; Vol. *237*, pp 323−369.
(42) Holmer, M.; Storkholm, P. Sulphate reduction and sulphur cycling in lake sediments: A review. *Freshwater Biol.* **2001**, *46*, 431−451.
(43) Rickard, D. Sedimentary Sulfides. In *Developments in Sedimentology*; Rickard, D., Ed.; Elsevier Ltd.: Oxford, UK, 2012; Vol. *65*, pp 543−604.
(44) Prietzel, J.; Thieme, J.; Neuhäusler, U.; Susini, J.; Kögel-Knabner, I. Speciation of sulphur in soils and soil particles by X-ray spectromicroscopy. *Eur. J. Soil Sci.* **2003**, *54*, 423−433.

(45) Rickard, D.; Morse, J. W. Acid volatile sulfide (AVS). *Mar. Chem.* **2005**, *97*, 141−197.
(46) Shakeri Yekta, S.; Gustavsson, J.; Svensson, B. H.; Skyllberg, U. Sulfur K-edge XANES and acid volatile sulfide analyses of changes in chemical speciation of S and Fe during sequential extraction of trace metals in anoxic sludge from biogas reactors. *Talanta* **2012**, *89*, 470−477.
(47) Lombi, E.; Hettiarachchi, G. M.; Scheckel, K. G. Advanced in situ spectroscopic techniques and their applications in Environmental Biogeochemistry: Introduction to the special section. *J. Environ. Qual.* **2011**, *40*, 659−666.
(48) Mayhew, L. E.; Webb, S. M.; Templeton, A. S. Microscale imaging and identification of Fe speciation and distribution during fluid−mineral reactions under highly reducing conditions. *Environ. Sci. Technol.* **2011**, *45*, 4468−4474.
(49) Lam, P. J.; Ohnemus, D. C.; Marcus, M. A. The speciation of marine particulate iron adjacent to active and passive continental margins. *Geochim. Cosmochim. Acta* **2012**, *80*, 108−124.
(50) Toner, B. M.; Marcus, M. A.; Edwards, K. J.; Rouxel, O.; German, C. R. Measuring the form of iron in hydrothermal plume particles. *Oceanography* **2012**, *25*, 209−212.
(51) Fliegel, D.; Knowles, E.; Wirth, R.; Templeton, A. S.; Staudigel, H.; Muehlenbachs, K.; Furnes, H. Characterization of alteration textures in Cretaceous oceanic crust (pillow lava) from the N-Atlantic (DSDP Hole 418A) by spatially-resolved spectroscopy. *Geochim. Cosmochim. Acta* **2012**, *96*, 80−93.
(52) Marcus, M. A.; MacDowell, A. A.; Celestre, R.; Manceau, A.; Miller, T.; Padmore, H. A.; Sublett, R. E. Beamline 10.3.2 at ALS: A hard X-ray microprobe for environmental and materials sciences. *J. Synchrotron Radiat.* **2004**, *11*, 239−247.
(53) Manceau, A.; Marcus, M. A.; Tamura, N., Quantitative speciation of heavy metals in soils and sediments by synchrotron X-ray techniques. In *Applications of Synchrotron Radiation in Low-Temperature Geochemistry and Environmental Science*; Fenter, P. A., Rivers, M. L., Sturchio, N. C., Sutton, S. R., Eds.; Mineralogical Society of America: Washington, DC, 2002; Vol. *49*, pp 341−428.
(54) Burton, E. D.; Bush, R. T.; Sullivan, L. A.; Hocking, R. K.; Mitchell, D. R. G.; Johnston, S. G.; Fitzpatrick, R. W.; Raven, M.; McClure, S.; Jang, L. Y. Iron-monosulfide oxidation in natural sediments: Resolving microbially mediated S transformations using XANES, electron microscopy, and selective extractions. *Environ. Sci. Technol.* **2009**, *43*, 3128−3134.
(55) Manceau, A.; Nagy, K. L. Quantitative analysis of sulfur functional groups in natural organic matter by XANES spectroscopy. *Geochim. Cosmochim. Acta* **2012**, *99*, 206−223.
(56) Webb, S. M. SIXpack: A graphical user interface for XAS analysis using IFEFFIT. *Phys. Scr.* **2005**, *2005*, 1011−1014.
(57) Toner, B. M.; Manceau, A.; Webb, S. M.; Sposito, G. Zinc sorption to biogenic hexagonal-birnessite particles within a hydrated bacterial biofilm. *Geochim. Cosmochim. Acta* **2006**, *70*, 27−43.
(58) Malinowski, E. R. Determination of the number of factors and the experimental error in a data matrix. *Anal. Chem.* **1977**, *49*, 612−617.
(59) Malinowski, E. R. Theory of error for target factor analysis with applications to mass spectrometry and nuclear magnetic resonance spectrometry. *Anal. Chim. Acta* **1978**, *103*, 339−354.
(60) Beauchemin, S.; Hesterberg, D.; Beauchemin, M. Principal component analysis approach for modeling sulfur K-XANES spectra of humic acids. *Soil Sci. Soc. Am. J.* **2002**, *66*, 83−91.
(61) Marcus, M. A.; Westphal, A. J.; Fakra, S. C. Classification of Fe-bearing species from K-edge XANES data using two-parameter correlation plots. *J. Synchrotron Radiat.* **2008**, *15*, 463−468.
(62) Prietzel, J.; Botzaki, A.; Tyufekchieva, N.; Brettholle, M.; Thieme, J.; Klysubun, W. Sulfur speciation in soil by S K-edge XANES spectroscopy: Comparison of spectral deconvolution and linear combination fitting. *Environ. Sci. Technol.* **2011**, *45*, 2878−2886.
(63) Marcus, M. A. X-ray photon-in/photon-out methods for chemical imaging. *TrAC, Trends Anal. Chem.* **2010**, *29*, 508−517.
(64) Zeng, T.; Arnold, W. A. Pesticide photolysis in prairie potholes: Probing photosensitized processes. *Environ. Sci. Technol.* **2013**, DOI: 10.1021/es3030808.
(65) Lovley, D. R.; Klug, M. J. Model for the distribution of sulfate reduction and methanogenesis in freshwater sediments. *Geochim. Cosmochim. Acta* **1986**, *50*, 11−18.
(66) Sinke, A. J. C.; Cornelese, A. A.; Cappenberg, T. E.; Zehnder, A. J. B. Seasonal variation in sulfate reduction and methanogenesis in peaty sediments of eutrophic Lake Loosdrecht, the Netherlands. *Biogeochemistry* **1992**, *16*, 43−61.
(67) Ziegelgruber, K. L. *Sediment Pore Water Dissolved Organic Matter in North Dakota (USA) Prairie Wetlands*; M.S. Thesis, The Ohio State University, Columbus, OH, 2011.
(68) Abdollahi, H.; Nedwell, D. B. Seasonal temperature as a factor influencing bacterial sulfate reduction in a saltmarsh sediment. *Microb. Ecol.* **1979**, *5*, 73−79.
(69) Howarth, R. W.; Teal, J. M. Sulfate reduction in a New England salt marsh. *Limnol. Oceanogr.* **1979**, *24*, 999−1013.
(70) Troelsen, H.; Jørgensen, B. B. Seasonal dynamics of elemental sulfur in two coastal sediments. *Estuar. Coast. Shelf Sci.* **1982**, *15*, 255−266.
(71) Westrich, J. T.; Berner, R. A. The effect of temperature on rates of sulfate reduction in marine sediments. *Geomicrobiol. J.* **1988**, *6*, 99−117.
(72) Leonard, E.; Mattson, V.; Benoit, D.; Hoke, R.; Ankley, G. Seasonal variation of acid volatile sulfide concentration in sediment cores from three northeastern Minnesota lakes. *Hydrobiologia* **1993**, *271*, 87−95.
(73) Moeslundi, L.; Thamdrup, B.; Jørgensen, B. B. Sulfur and iron cycling in a coastal sediment: Radiotracer studies and seasonal dynamics. *Biogeochemistry* **1994**, *27*, 129−152.
(74) Panutrakul, S.; Monteny, F.; Baeyens, W. Seasonal variations in sediment sulfur cycling in the Ballastplaat mudflat, Belgium. *Estuaries Coasts* **2001**, *24*, 257−265.
(75) Al-Raei, A. M.; Bosselmann, K.; Bottcher, M. E.; Hespenheide, B.; Tauber, F. Seasonal dynamics of microbial sulfate reduction in temperate intertidal surface sediments: Controls by temperature and organic matter. *Ocean Dynam* **2009**, *59*, 351−370.
(76) Jørgensen, B. B. The sulfur cycle of a coastal marine sediment (Limfjorden, Denmark). *Limnol. Oceanogr.* **1977**, *22*, 814−832.
(77) Sørensen, J.; Jeørgensen, B. B. Early diagenesis in sediments from Danish coastal waters: Microbial activity and Mn−Fe−S geochemistry. *Geochim. Cosmochim. Acta* **1987**, *51*, 1583−1590.
(78) King, G. M. Patterns of sulfate reduction and the sulfur cycle in a South Carolina salt marsh. *Limnol. Oceanogr.* **1988**, *33*, 376−390.
(79) Dacey, J. W. H.; Howes, B. L. Water uptake by roots controls water table movement and sediment oxidation in short *Spartina* marsh. *Science* **1984**, *224*, 487−489.
(80) Morris, J. T.; Whiting, G. J. Gas advection in sediments of a South Carolina salt marsh. *Mar. Ecol.: Prog. Ser.* **1985**, *27*, 187−194.
(81) Luther, G. W., III; Church, T. M. Seasonal cycling of sulfur and iron in porewaters of a Delaware salt marsh. *Mar. Chem.* **1988**, *23*, 295−309.
(82) Thamdrup, B.; Finster, K.; Fossing, H.; Hansen, J. W.; Jørgensen, B. B. Thiosulfate and sulfite distributions in porewater of marine sediments related to manganese, iron, and sulfur geochemistry. *Geochim. Cosmochim. Acta* **1994**, *58*, 67−73.
(83) Bostick, B. C.; Theissen, K. M.; Dunbar, R. B.; Vairavamurthy, M. A. Record of redox status in laminated sediments from Lake Titicaca: A sulfur K-edge X-ray absorption near edge structure (XANES) study. *Chem. Geol.* **2005**, *219*, 163−174.
(84) Toevs, G. R.; Morra, M. J.; Polizzotto, M. L.; Strawn, D. G.; Bostick, B. C.; Fendorf, S. Metal(loid) diagenesis in mine-impacted sediments of Lake Coeur d'Alene, Idaho. *Environ. Sci. Technol.* **2006**, *40*, 2537−2543.
(85) Morgan, B.; Burton, E. D.; Rate, A. W. Iron monosulfide enrichment and the presence of organosulfur in eutrophic estuarine sediments. *Chem. Geol.* **2012**, *296*−*297*, 119−130.

(86) Eglinton, T. I.; Irvine, J. E.; Vairavamurthy, A.; Zhou, W.; Manowitz, B. Formation and diagenesis of macromolecular organic sulfur in Peru margin sediments. *Org. Geochem.* **1994**, *22*, 781−799.
(87) Vairavamurthy, M. A.; Zhou, W.; Eglinton, T. I.; Manowitz, B. Sulfonates: A novel class of organic sulfur compounds in marine sediments. *Geochim. Cosmochim. Acta* **1994**, *58*, 4681−4687.
(88) Vairavamurthy, M. A.; Wang, S.; Khandelwal, B.; Manowitz, B.; Ferdelman, T.; Fossing, H. Sulfur transformations in early diagenetic sediments from the Bay of Conception, off Chile. In *Geochemical Transformations of Sedimentary Sulfur*; Vairavamurthy, M. A., Schoonen, M. A. A., Eglinton, T. I., Luther, G. W., III, Manowitz, B., Eds.; American Chemical Society: Washington, DC, 1995; Vol. *612*, pp 38−58.
(89) Rickard, D.; Luther, G. W., III Chemistry of iron sulfides. *Chem. Rev.* **2007**, *107*, 514−562.
(90) Anxolabéhère-Mallart, E.; Glaser, T.; Frank, P.; Aliverti, A.; Zanetti, G.; Hedman, B.; Hodgson, K. O.; Solomon, E. I. Sulfur K-edge X-ray absorption spectroscopy of 2Fe−2S ferredoxin: Covalency of the oxidized and reduced 2Fe forms and comparison to model complexes. *J. Am. Chem. Soc.* **2001**, *123*, 5444−5452.
(91) Dey, A.; Glaser, T.; Moura, J. J. G.; Holm, R. H.; Hedman, B.; Hodgson, K. O.; Solomon, E. I. Ligand K-edge X-ray absorption spectroscopy and DFT calculations on $[Fe_3S_4]^{0,+}$ clusters: Delocalization, redox, and effect of the protein environment. *J. Am. Chem. Soc.* **2004**, *126*, 16868−16878.
(92) Vairavamurthy, M. A.; Mopper, K. Geochemical formation of organosulphur compounds (thiols) by addition of H_2S to sedimentary organic matter. *Nature* **1987**, *329*, 623−625.
(93) Vairavamurthy, M. A.; Maletic, D.; Wang, S.; Manowitz, B.; Eglinton, T. I.; Lyons, T. Characterization of sulfur-containing functional groups in sedimentary humic substances by X-ray absorption near-edge structure spectroscopy. *Energy Fuels* **1997**, *11*, 546−553.
(94) Kiene, R. P.; Visscher, P. T. Production and fate of methylated sulfur compounds from methionine and dimethylsulfoniopropionate in anoxic salt marsh sediments. *Appl. Environ. Microbiol.* **1987**, *53*, 2426−2434.
(95) Kiene, R. P.; Malloy, K. D.; Taylor, B. F. Sulfur-containing amino acids as precursors of thiols in anoxic coastal sediments. *Appl. Environ. Microbiol.* **1990**, *56*, 156−161.
(96) Risberg, E. D.; Jalilehvand, F.; Leung, B. O.; Pettersson, L. G. M.; Sandstrom, M. Theoretical and experimental sulfur K-edge X-ray absorption spectroscopic study of cysteine, cystine, homocysteine, penicillamine, methionine and methionine sulfoxide. *Dalton Trans.* **2009**, 3542−3558.
(97) Schouten, S.; Eglinton, T. I.; Sinninghe Damsté, J. S.; de Leeuw, J. W., Influence of sulphur cross-linking on the molecular-size distribution of sulphur-rich macromolecules in bitumen. In *Geochemical Transformations of Sedimentary Sulfur*; Vairavamurthy, M. A., Schoonen, M. A. A., Eglinton, T. I., Luther, G. W., III, Manowitz, B., Eds.; American Chemical Society: Washington, DC, 1995; Vol. *612*, pp 80−92.
(98) van Dongen, B. E.; Schouten, S.; Baas, M.; Geenevasen, J. A. J.; Sinninghe Damsté, J. S. An experimental study of the low-temperature sulfurization of carbohydrates. *Org. Geochem.* **2003**, *34*, 1129−1144.
(99) Prietzel, J.; Thieme, J.; Tyufekchieva, N.; Paterson, D.; McNulty, I.; Kögel-Knabner, I. Sulfur speciation in well-aerated and wetland soils in a forested catchment assessed by sulfur K-edge X-ray absorption near-edge spectroscopy (XANES). *J. Plant Nutr. Soil Sci.* **2009**, *172*, 393−403.
(100) Pingitore, N. E., Jr.; Meitzner, G.; Love, K. M. Identification of sulfate in natural carbonates by X-ray absorption spectroscopy. *Geochim. Cosmochim. Acta* **1995**, *59*, 2477−2483.
(101) Myneni, S. C. B. X-ray and vibrational spectroscopy of sulfate in earth materials. *Rev. Mineral. Geochem.* **2000**, *40*, 113−172.
(102) Luther, G. W., III; Church, T. M. An overview of the environmental chemistry of sulphur in wetland systems. In *Sulphur Cycling on the Continents: Wetlands, Terrestrial Ecosystems, and Associated Water Bodies*; Howarth, R. W., Stewart, J. W. B., Ivanov, M. V., Eds.; SCOPE, John Wiley & Sons, Inc.: Somerset, NJ, 1992; pp 125−142.
(103) Schroth, A. W.; Bostick, B. C.; Graham, M.; Kaste, J. M.; Mitchell, M. J.; Friedland, A. J. Sulfur species behavior in soil organic matter during decomposition. *J. Geophys. Res.* **2007**, *112*, DOI 10.1029/2007JG000538.